Journal of Southeast University (English Edition) Vol. 42, No. 1, pp. 26-35 Mar. 2026 ISSN 1003-7985

An improved Alpha-shape algorithm for extracting section contours of the super-high steel bridge tower using point clouds

ZHANG Yiming, ZHAO Tianhao, LIAO Ruixuan, LI Haoqing, WANG Hao

(Key Laboratory of Concrete and Prestressed Concrete Structures of Ministry of Education, Southeast University, Nanjing 211189, China)

Abstract: The virtual preassembly of super-high steel bridge towers faces a challenge in the efficient and precise extraction of complex cross-sectional features. Factors such as fabrication errors, gravity-induced deformations, and temperature fluctuations can compromise the accuracy of contour extraction. To address these limitations, an improved Alpha-shape-based point cloud contour extraction method is proposed. The proposed approach uses a hierarchical strategy to process three-dimensional laser scanning point clouds. The processed data are then subjected to curvature-adaptive voxel filtering to reduce acquisition noise. In addition, an enhanced iterative closest point (ICP) variant with correspondence validation accurately aligns the discrete point cloud segments. The proposed curvature-responsive Alpha-shape framework enables multiscale contour delineation through topology-adaptive threshold modulation, which resolves boundary ambiguities in geometrically complex cross-sections. The method was experimentally validated using field-acquired measurement datasets from the Zhangjinggao Yangtze River Bridge tower segments, confirming its capability to reconstruct noncanonical cross-sectional geometries. Three contour extraction methods, including Poisson reconstruction, the conventional Alpha-shape algorithm, and random sample consensus with ICP (RANSAC-ICP), were compared to evaluate the performance of the proposed Alpha-shape algorithm. The results demonstrate that the proposed method achieves superior contour extraction accuracy and data reduction efficiency, highlighting its effectiveness in contour extraction tasks.

Key words: super-high steel bridge tower; point cloud; contour extraction; improved Alpha-shape algorithm

DOI: 10.3969/j.issn.1003-7985.2026.01.003

Received 2025-07-04, **Revised** 2025-10-22.

Biographies: ZHANG Yiming (1992—), male, doctor, professor; WANG Hao (corresponding author), male, doctor, professor, wanghao1980@seu.edu.cn.

Foundation items: The National Natural Science Foundation of China (No. 52338011), the Start-up Research Fund of Southeast University (No. RF1028624058), the Southeast University Interdisciplinary Research Program for Young Scholars, the National Key Research and Development Program of China (No. 2024YFC3014103).

Citation: ZHANG Yiming, ZHAO Tianhao, LIAO Ruixuan, et al. An improved Alpha-shape algorithm for extracting section contours of the super-high steel bridge tower using point clouds[J]. Journal of Southeast University (English Edition), 2026, 42(1): 26-35. DOI: 10.3969/j.issn.1003-7985.2026.01.003.

Steel bridge towers are indispensable load-bearing components in bridge engineering, particularly with the trend toward super-long configurations and increasingly complex structural systems. This prominence stems from their exceptional properties, including high strength-to-weight ratios, ease of assembly, and superior seismic performance[1]. However, during the fabrication and erection phases, steel tower segments are susceptible to dimensional deviations, gravity-induced deformations, and environmental influences. Traditional pre-erection alignment methods also have limitations, such as large spatial requirements, inefficient multisystem coordination, and variability in accuracy from manual operations[2]. These constraints usually increase the risk of delays in long-span bridge construction[3].

To address the limitations of traditional alignment methods, point cloud-based virtual preassembly simulation has emerged as an innovative digital solution. This technique uses three-dimensional (3D) laser scanning to capture high-density point cloud data of segment surfaces, enabling noncontact assembly simulations. The spatial constraints and inefficiencies associated with physical preassembly processes are eliminated. For instance, Rebolj et al. [4] proposed a geometric quality assessment method that combines 3D laser scanning with building information modeling (BIM). By integrating this approach with Scan-vs-BIM techniques, geometric deviations were effectively detected, and on-site assembly errors were significantly reduced. Zhou et al. [5] developed a virtual preassembly method for steel arch bridges using point cloud data by applying control point extraction based on random sample consensus (RANSAC) and Hough transform algorithms. Similarly, Zhu et al. [6] introduced a virtual preassembly algorithm for steel-box segments using the point cloud library, employing statistical filtering and iterative closest point (ICP) registration to automate the fit evaluation between adjacent segments. However, steel bridge towers usually have irregular cross-sections, making them more susceptible to point cloud artifacts and uneven point distribution. Furthermore, current computational methods often rely on rigid parameter tuning, which struggles to balance global shape continuity with fine detail accuracy

in multiscale analysis.

The Alpha-shape algorithm, which is particularly effective for handling nonuniform geometries, is widely used for geometric feature extraction in point cloud analysis. Based on Delaunay triangulation, its adaptive edge delineation framework enables flexible boundary reconstruction regardless of topology. Cheng et al. [7] enhanced sparse point cloud feature extraction using layered slicing and dynamic α-values adjustments; however, their method suffered from detail loss in high-curvature regions[8]. Santos et al. [9] introduced a locally adaptive Alpha-shape approach that adjusts edge parameters based on local point spacing. However, the reliance of the method on predefined neighborhood radii can cause instability when applied to datasets with extreme density variations or fine structural features. Zang et al. [10] proposed a dual-threshold Alpha-shape framework that combines coarse-to-fine edge extraction using complementary α-values, along with least-squares contour regularization. Although this approach balances completeness and precision better than single-threshold methods, its fixed α-pairing limits adaptability to irregular geometries, such as nonorthogonal joints or multiscale structural elements. Conventional Alpha-shape methods are limited by rigid parameterization, which prevents adaptation across diverse structural types and often tradeoff between flexibility and feature extraction accuracy[11].

This study proposes an improved Alpha-shape algorithm that incorporates boundary grid-weighted optimization and dynamic layered α-values iteration to extract complex geometric features from steel bridge tower segments with high fidelity. First, a denoising framework based on Euclidean clustering and *K*-dimensional tree (KD-tree) indexing is employed to improve feature stability under high-noise conditions. Second, a curvature-driven multiscale α-values adaptation method is introduced to simultaneously capture both fine details and global contours. Subsequently, a corner matching error propagation model based on extremum analysis is established to quantitatively assess alignment deviations during segment assembly. Finally, the proposed method is validated using point cloud data from the super-high tower sections of the Zhangjinggao Yangtze River Bridge (ZYRB), confirming its effectiveness in real-world engineering scenarios.

1 Point Cloud-Based Section Contour Extraction Framework

This study proposes a point cloud-based section contour extraction framework with adaptive multiscale features to significantly improve the accuracy of contour reconstruction for irregular steel structural sections. This framework comprises four parts: scanning scheme design, point cloud preprocessing, planar extraction, and Alpha-shape-based contour extraction. The flowchart is shown in Fig. 1.

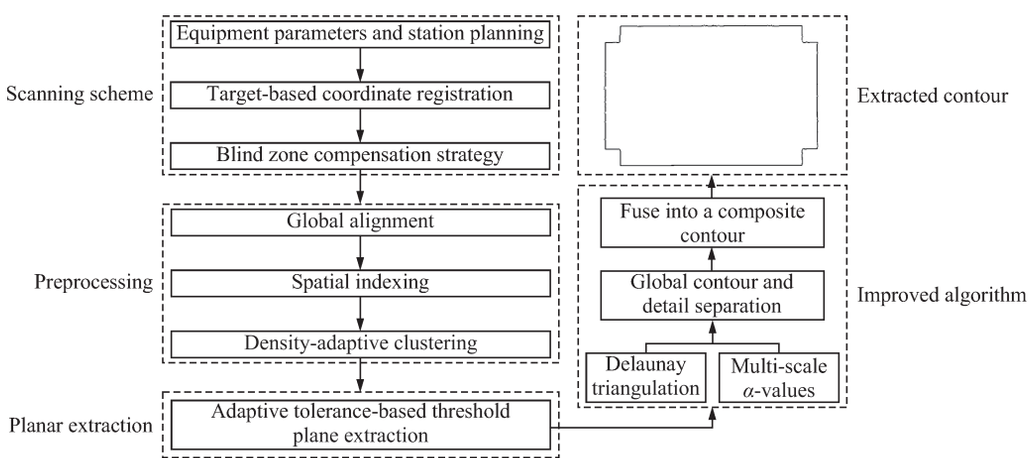

Fig. 1 Flowchart of point cloud-based section contour extraction

As shown in Fig. 1, a FARO Focus Core terrestrial laser scanner acquires holographic geometry data for the steel bridge tower segments, and a three-target co-visibility method establishes interstation coordinate transformations. For unscannable areas at segment-ground interfaces, handheld scanning combined with ICP fusion supplements critical feature lines. The preprocessing procedure for efficient noise reduction comprises three phases: global alignment, spatial indexing, and density-adaptive clustering. Adaptive tolerance-based threshold plane extraction generates a two-dimensional (2D) planar dataset. Finally, the contours are extracted using the Alpha-shape-based algorithm, which creates equivalent Alpha-shape contours by employing a defined set of multiscale α-values $\{\alpha_1, \alpha_2, \cdots, \alpha_n\}$.

2 Segment Modeling of Bridge Towers Using 3D Laser Scanning

2.1 Scanning scheme design and optimization

A 3D laser scanning technology, featuring multiperspective observation and real-scene reconstruction capa-

bilities, efficiently acquires comprehensive geometric data for steel bridge tower segments[12]. A systematic scanning approach is used as follows:

(1) Equipment parameters and station planning

Point cloud data are acquired using a FARO Focus Core terrestrial laser scanner, with a ranging accuracy of ±2 mm @ 10 m and a scanning rate of 9.76 ×10^5 points per second. A multistation coverage strategy is designed based on segment dimensions. Stations are deployed at 5-m intervals along the longitudinal axis of the segment to ensure a minimum 30% overlap between adjacent stations. The four corners of the tower segment are supported on steel members with a height of no more than 1 m to ensure stability and maintain the segment at the same horizontal level as the ground. Four terrestrial laser scanners are positioned around the tower segment, with elevation angles set between 30° and 60° to optimize point cloud density and ensure a point spacing of no more than 2 mm.

(2) Target-based coordinate registration

Spherical targets (100 mm diameter, 80% reflectivity) are deployed in the transitional zones between adjacent stations, with a spacing not exceeding 1/3 of the segment width (approximately 2.7 m). A three-target co-visibility method is used to establish interstation coordinate transformations. After verification using on-site time-of-flight measurements, the average registration accuracy of multistation point cloud alignment was approximately 2.45 mm.

(3) Blind zone compensation strategy

For unscannable areas at segment-ground interfaces (approximately 0.5 m in height), a dual-phase data repair technique is implemented. First, the spatial interpolation of adjacent station point clouds is used to generate the initial surface geometry. Second, mobile handheld scanning (with an accuracy of ±0.05 mm) is used to supplement the critical feature lines. To enhance local registration accuracy, several target points are arranged around the bolted holes of the segment, and local cloud fusion using ICP algorithms reconstructs complete surface models.

2.2 Point cloud preprocessing

The acquired point cloud data of super-high steel bridge towers typically contain between 5% and 8% outlier noise due to environmental interference and equipment errors, directly compromising contour extraction and virtual assembly accuracy. A three-phase denoising framework is proposed to efficiently reduce noise while preserving critical features[13-14] (Fig. 2).

Fig. 2 Flowchart of point cloud preprocessing for segment preassembly

For multistation point cloud data, a target-based coordinate system mapping method is adopted to transform local coordinate systems into a global world coordinate system

$$\boldsymbol{P}_{\text{world}} = \boldsymbol{R}\boldsymbol{P}_{\text{local}} + \boldsymbol{T} \tag{1}$$

where $\boldsymbol{P}_{\text{world}}$ represents points in the transformed world coordinate system; $\boldsymbol{P}_{\text{local}}$ represents the original local coordinates of point cloud data; $\boldsymbol{R}$ represents the rotation matrix; and $\boldsymbol{T}$ represents the translation vector.

Subsequently, a KD-tree-based spatial indexing structure[11] is constructed. A KD-tree node can be split into two subspaces using a hyperplane, and each subspace can be split recursively in the same manner. Every subspace is separated into left and right subspaces. A KD-tree is a space-partitioning data structure that organizes points in a K-dimensional space. Each node in the tree represents a distinct, K-dimensional rectangular region.

To mitigate clustering bias stemming from random seed initialization, this study develops a density-based seed optimization strategy comprising three sequential steps. First, the local point concentration is quantified using Gaussian kernel density estimation by calculating the density at point i through radial basis weighting of neighboring points within the feature space. Second, based on the density distribution, an adaptive search radius technique creates a baseline radius of $r = 3\sigma_p$ (three standard deviations of point density) and applies exponential decay modulation around local density extremes to dynamically scale the neighborhood query range. Finally, KD-tree accelerated metric computation is used to precisely evaluate spatial closeness, guaranteeing effec-

tive cluster border determination:

$$\rho_i = \sum_{j=1}^{k} \exp\left(-\frac{d_{ij}^2}{2\sigma_p^2}\right) \tag{2}$$

$$r_i = 3\sigma_p\left(1 + 0.5\frac{\rho_{max} - \rho_i}{\rho_{max}}\right) \tag{3}$$

$$d_{ij} = \sqrt{(x_i - x_j)^2 + (y_i - y_j)^2 + (z_i - z_j)^2} \tag{4}$$

where d_{ij} denotes the Euclidean distance between points i and j; σ_p denotes the standard deviation of point cloud density; and (x_i, y_i, z_i) and (x_j, y_j, z_j) denote the 3D coordinates of the two points.

Points satisfying $d_{ij} \leqslant r$ are classified into the same cluster, and their visited status is updated to prevent redundant processing[15]. The neighborhood search is accelerated by leveraging the preconstructed spatial indexing structure, and the identified neighboring points are assigned to the current cluster. This iterative process continues until no new neighborhood points are detected. Upon cluster completion, new seed points are stochastically selected from unvisited points, and the procedure repeats until all points are processed, thereby finalizing the clustering workflow.

2.3 Planar feature extraction and optimization

2.3.1 Conventional method

The traditional RANSAC algorithm estimates planar models using random sampling consensus[14]:

$$ax + by + cz + d = 0 \tag{5}$$

The number of its iteration times, T, and the inlier rate ω satisfy

$$T = \frac{\log(1 - p)}{\log(1 - \omega^t)} \tag{6}$$

where $t = 3$ denotes the minimum sample number and $p = 0.99$ represents the confidence probability. For a model with a point cloud size of 16×10^6 points and an inlier rate of $\omega = 85\%$, the process required up to 573 iterations and 42 min to complete. This process is highly susceptible to local noise interference, which often results in the generation of pseudo-planes.

2.3.2 Adaptive tolerance-based threshold plane extraction

(1) Analysis of point cloud spatial dispersion

Z-coordinate profiling is used to statistically characterize the point cloud vertical distribution before beginning the spatial dispersion analysis. This involves calculating the central tendency and variability metrics of the elevation data. The vertical centroid measures the average height position and represents the degree of elevation fluctuation throughout the scanned structure. Adaptive thresholding, which dynamically calibrates the tolerance band in proportion to localized point concentration patterns, is based on these statistical underpinnings to create intelligent screening criteria for upper surface identification. The following is an expression for the guiding computations:

$$\mu_z = \frac{1}{n}\sum_{i=1}^{n} z_i, \quad \sigma_z = \sqrt{\frac{1}{n-1}\sum_{i=1}^{n}(z_i - \mu_z)^2} \tag{7}$$

$$z_i \geqslant \mu_z + 2\sigma_z - \Delta z \tag{8}$$

where μ_z denotes the mean of the Z-coordinates; σ_z denotes the standard deviation; and Δz denotes the tolerance threshold, which can be dynamically adjusted according to the point cloud density.

(2) Plane optimization and projection

The candidate point set undergoes radius filtering using the KD-tree ($r = 5\sigma_z$) to remove isolated noise points. The optimal plane equation is solved to minimize the projection error as follows:

$$\min \sum_{i=1}^{m}(ax_i + by_i + cz_i + d)^2 \tag{9}$$

The planar point cloud is projected onto the XY coordinate system to generate a 2D contour dataset.

3 Improved Alpha-shape for Point Cloud Contour Extraction

3.1 Improved Alpha-shape algorithm

In the virtual assembly of steel bridge towers, the accuracy of contour extraction directly affects the reliability of segment matching. Unlike traditional convex hull algorithms, the Alpha-shape algorithm flexibly accommodates complex geometries and multiple topological structures[10]. The α-value parameter is adjusted to control the level of detail and smoothness in the generated contour. The generation process is as follows.

Step 1 Neighborhood graph construction: starting from a given point set $P = \{P_1, P_2, \cdots, P_n\}$, calculate the neighborhood of each point, typically by computing the Euclidean distances between points to construct the graph.

Step 2 Circumcircle construction: for three points (in 2D space) P_i, P_j, $P_k \subseteq P$, their circumcircle is defined as

$$C_{ijk} = C(P_i, P_j, P_k) \tag{10}$$

where $C(P_i, P_j, P_k)$ denotes the circumcenter of the triangle formed by points P_i, P_j, P_k.

If the radius r_{ijk} of this circumcircle is less than a given parameter α-value, the points lie on the contour edge as follows:

$$r_{ijk} < \alpha \quad (P_i, P_j, P_k) \in \text{Alpha-shape} \tag{11}$$

Step 3 Contour extraction: qualified points and edges are selected to extract an external contour with topological features.

Fig. 3 illustrates the application of the Alpha-shape algorithm to point cloud data. The black points represent

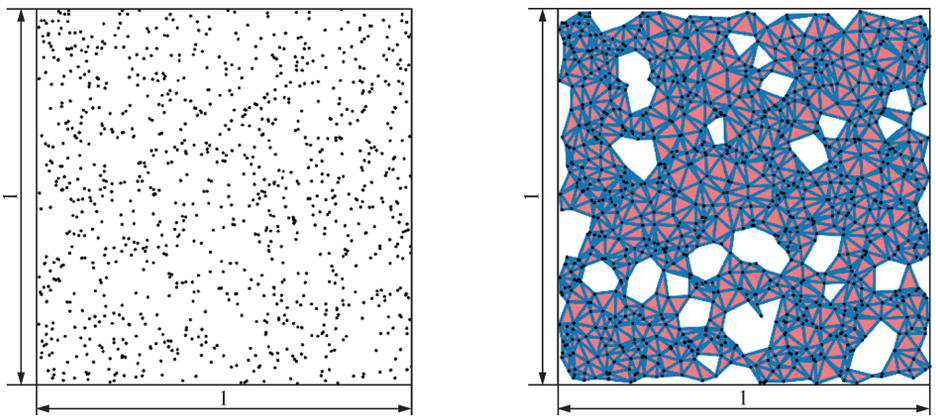

Fig. 3 Comparison diagram of Alpha-shape results for point cloud data (unit: m). (a) Data; (b) α_{opt}

discretely distributed point cloud that randomly generated within a 1 m×1 m region (Fig. 3(a)). The Alpha-shape Panel (highlighted in blue) shows the reconstructed boundary generated using an optimized α-value (α_{opt}) (Fig. 3(b)). Internal red triangular regions are generated via Delaunay triangulation[16]. A triangle is identified as a contour feature if its circumcircle radius is less than the specific α-value.

This study employs multiscale α-values to capture point cloud geometric features across varying scales. The complete flowchart of the improved algorithm is shown in Fig. 4.

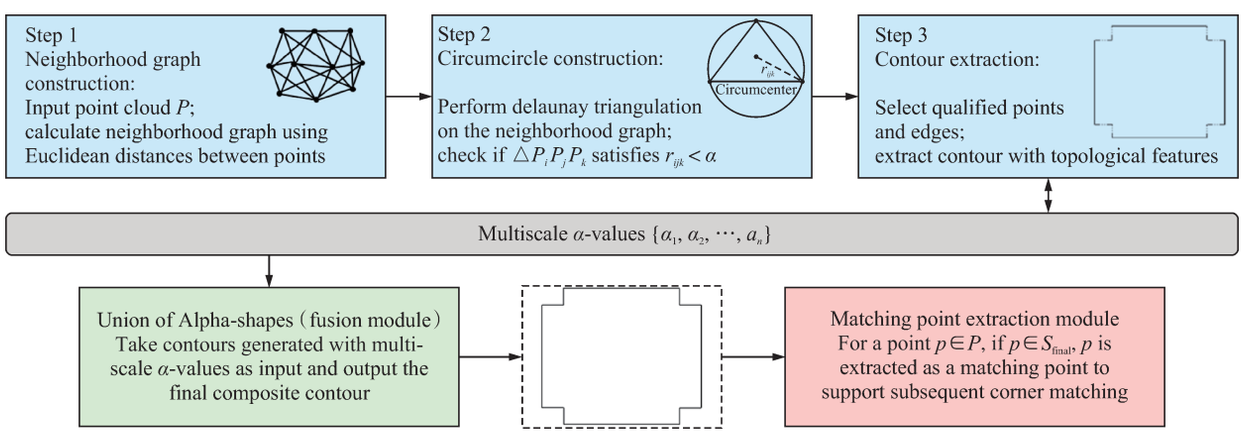

Fig. 4 Flowchart of the improved Alpha-shape algorithm

A set of multiscale α-values $\{\alpha_1, \alpha_2, \cdots, \alpha_n\}$ is defined, each generating corresponding Alpha-shape contours as follows:

$$S_{\alpha_i} = \text{Alpha-shape}(P, \alpha_i) \quad i = 1, 2, \cdots, n \tag{12}$$

where α_i denotes the contour tightness coefficient controlling geometric granularity.

The multiscale Alpha-shape results are fused into a composite contour via a unary union operation. The fused geometric object is expressed as

$$S_{\text{merged}} = \bigcup_{i=1}^{n} \text{Boundary}\left(S_{\alpha_i}\right) \tag{13}$$

where $\cup$ denotes the geometric union operator and S_{merged} denotes the fused composite contour.

For a given point $p = (x, y) \in P$, the matching criterion is defined such that a point is considered a match if it either belongs to S_{final} or is close enough to be regarded as touching S_{final}. The points meeting this criterion are extracted and identified as matching points to facilitate subsequent corner matching processes.

The contour point matching criteria are defined as follows: for any point $p_j \in S$, it is classified as a valid contour point if it satisfies

$$\exists p_k \in S_{\text{merged}}, \quad \| p_j - p_k \|_2 \leqslant \delta \tag{14}$$

where p_k denotes a reference point in S_{merged}.

3.2 Corner matching and assembly error quantification

3.2.1 Extremum-based corner detection

Based on each extracted contour points (x_i, y_i), the coordinates of four feature corners, denoted as p_{T_L} (top left), p_{B_L} (bottom left), p_{T_R} (top right), p_{B_R} (bottom right), are localized using a modified extremum method as follows:

$$p_{T\_L} = \underset{p_i \in S_{\text{merged}}}{\arg\min} (x_i - \gamma y_i) \tag{15}$$

$$p_{\mathrm{B\_R}} = \arg\max_{p_i \in S_{\mathrm{merged}}} (x_i + \gamma y_i) \tag{16}$$

$$p_{\mathrm{T\_R}} = \arg\max_{p_i \in S_{\mathrm{merged}}} (x_i + \gamma y_i) \tag{17}$$

$$p_{\mathrm{B\_R}} = \arg\min_{p_i \in S_{\mathrm{merged}}} (x_i - \gamma y_i) \tag{18}$$

where $\gamma = 0.01$ is the weighting coefficient used to balance dimensional discrepancies between coordinate axes.

3.2.2 Assembly error propagation analysis

The corner sets are defined as $c = \{p_{\mathrm{T\_L}}, p_{\mathrm{B\_L}}, p_{\mathrm{T\_R}}, p_{\mathrm{B\_R}}\}$. Let the set of points extracted from the upper surface of one segment be denoted as c_1, and those from the lower surface of another segment be denoted as c_2. For c_1 and c_2, the error metrics between the corresponding corners are computed. The Euclidean norm[16] is used to quantify the differences between the structural corners. For the m-th corner C_{1m} in c_1 and its corresponding corner C_{2m} in c_2, the corner errors are calculated as follows:

$$E_m = \| C_{1m} - C_{2m} \| = \sqrt{(x_1^2 - x_2^2) - (y_1^2 - y_2^2)} \tag{19}$$

The errors for all four corner points are calculated individually and aggregated into an error metrics array[17]. This approach intuitively evaluates the similarity or dissimilarity in corner features between corners$_1$ and corners$_2$ by quantifying positional differences between adjacent corners into concrete error values[18].

3.3 Evaluation metrics

Four criteria, including contour completeness (C_{comp}), Hausdorff distance (D_{H}), maximum processable points ($N_{\max}$), and contour similarity index (C_{SI}), are employed to evaluate the performance advantage of the improved algorithm. The evaluation principle is that better contour extraction results in smaller D_{H} and higher C_{comp}, $N_{\max}$, and C_{SI}. The criteria are defined as follows[19].

(1) Contour completeness (C_{comp})

This metric quantifies the coverage of extracted contours relative to the original point cloud and is calculated as follows:

$$C_{\mathrm{comp}} = \frac{1}{|P|} \sum_{p \in P} I(d(p, C) \leqslant \varepsilon) \times 100\% \tag{20}$$

where $|P|$ denotes the total number of points; C denotes the extracted contour point set; $d(p, C)$ denotes the minimum Euclidean distance from point p to contour C; ε denotes the tolerance threshold; and $I(\cdot)$ denotes the indicator function.

(2) Hausdorff distance (D_{H})

This metric quantifies the maximum approximation error between the two datasets and is defined as follows:

$$D_{\mathrm{H}}(A, B) = \max\left(\sup_{a \in A} \inf_{b \in B} \| a - b \|, \sup_{b \in B} \inf_{a \in A} \| b - a \| \right) \tag{21}$$

where A denotes the algorithm-extracted contour point dataset and B denotes the ground-truth contour point dataset.

(3) Maximum processable points ($N_{\max}$)

This metric represents the maximum point cloud scale an algorithm can effectively process, typically constrained by memory and computational time. $N_{\max}$ is defined as

$$N_{\max} = \max\{N \mid O(N) \leqslant O_{\mathrm{limit}}\} \tag{22}$$

where $O(N)$ denotes processing time for a point cloud of size N; O_{limit} denotes allowable time.

(4) Contour similarity index(C_{SI})

This metric quantifies the similarity between the extracted and ground-truth contours by combining the overlap ratio and normalized average distance

$$C_{\mathrm{SI}} = \frac{R}{1 + D} = \frac{\dfrac{1}{|C| + |P|}\left(\sum_{c \in C} I(d(c, P) \leqslant D) + \sum_{p \in P} I(d(p, C) \leqslant D) \right)}{1 + \dfrac{1}{2}\left(\dfrac{1}{|C|} \sum_{c \in C} d(c, P) + \dfrac{1}{|P|} \sum_{p \in P} d(p, C) \right)} \tag{23}$$

where R represents the overlap ratio, and D represents the average minimum distance(AMD) defined as the average of the mean distances between contours C and P.

4 Case Study

4.1 Point cloud data acquisition of ZYRB

The main tower of the ZYRB uses a hybrid structural system of steel-box girders and concrete-filled steel tubes, with a total height of 328.5 m. The tower is vertically divided into 24 prefabricated segments (FTN1-FTN24) and horizontally into four chamber units (HL1-HL4) (Fig. 5)[20], where HL denotes a beam segment, FT denotes a tower segment, and the letters following FT

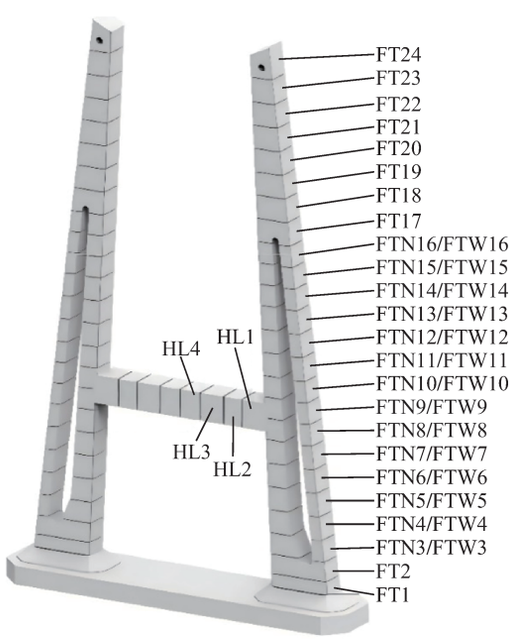

Fig. 5 Schematic of bridge tower segment distribution

indicate position (N for inside and W for outside). A typical segment measures 12.6 m in length, 8.4 m in width, and 6.0 m in height.

Data acquisition was performed using a FARO Focus S 350 laser scanner (with ranging accuracy of ±1 mm at 25 m) under a multistation collaborative scanning protocol.

Four terrestrial laser scanners were positioned around the tower segment, with elevation angles set between 30° and 60°. Using a resolution of 1 600 dpi and a station scanning duration of 15 min, the configuration achieved a point spacing below 2 mm, meeting the millimeter-level dimensional fidelity requirement. High-reflectivity spherical targets (100-mm diameter, labeled T1-T6) were strategically positioned in overlapping zones with a maximum spacing of 2.7 m to achieve submillimeter registration accuracy through three-target co-visibility verification. A handheld Artec Leo scanner (range accuracy of ±0.05 mm) was used to capture the critical contact-zone feature lines. The complete surface models were reconstructed by fusing local point clouds using ICP methods.

4.2 Point cloud preprocessing and surface extraction

The original point cloud datasets for segments FTN12-FTN14 acquired by the scanner contain 26.119×10^6, 29.520×10^6, and 19.912×10^6 points, respectively. Fig. 6(a) shows the initial point cloud of FTN13 obtained using a terrestrial laser scanner. Unavoidable noise points surround the critical geometric features. The proposed Euclidean cluster segmentation algorithm was used to denoise the FTN13 segment (Fig. 6(b)). With a noise removal rate of 46.3%, the point cloud size shrank to 15.829×10^6 points after postprocessing.

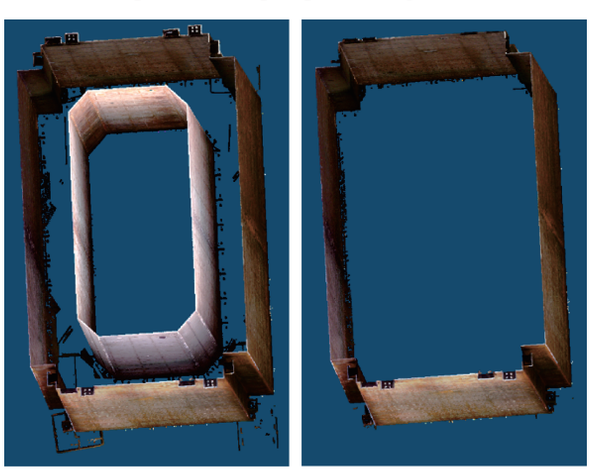

(a) (b)

Fig. 6 FTN13 point cloud data. (a) Before treatment; (b) After treatment

The virtual assembly reference is established through a three-stage computational geometry surface extraction process applied to denoised point clouds. First, vertical coordinate analysis identifies upper surface candidates using statistical threshold filtering, retaining points that meet the elevation condition $z_i \geqslant z_{\max} - \Delta z$ through Z-axis extremum analysis. Second, planar surface reconstruction applies a density-weighted optimization, where least-squares weighting coefficients are dynamically assigned $\omega_i = 1.5$ for high-density regions and $\omega_i = 0.5$ for low-density zones, ensuring preferential fitting accuracy in structurally critical areas. Finally, dimensional abstraction is achieved by projecting the 3D planar point set into a 2D coordinate system, generating the millimeter-precise contour representations (Fig. 7).

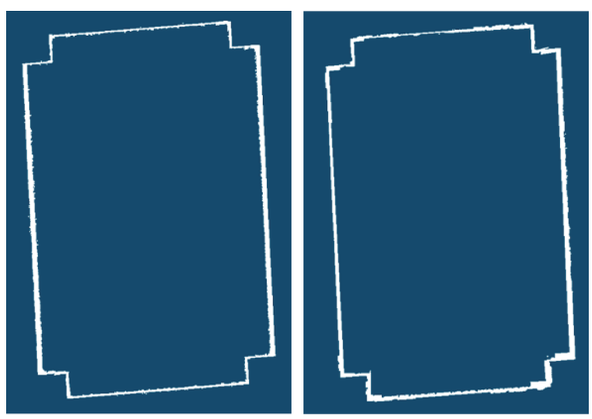

(a) (b)

Fig. 7 Surface point cloud data. (a) FTN13 surface point cloud data; (b) FTN14 lower surface point cloud data

4.3 Contour extraction using the proposed method

Contour extraction is performed on the processed planar surfaces using both conventional Alpha-shape algorithms and the proposed multiscale alpha fusion method to generate closed boundaries.

Fig. 8 shows a notable advancement in geometric feature preservation achieved by the improved algorithm over its conventional counterpart. The static parameterization of conventional Alpha-shape approaches causes incomplete capture of irregular corner geometries, particularly at microstructural transitions (Fig. 8(b)). In contrast, the improved method overcomes this constraint through density-adaptive alpha selection (Fig. 8(c)). This multiscale boundary reconstruction is based on local point concentration: higher α values stabilize the global contour, whereas lower values preserve fine features.

Controlled benchmark testing confirms that this dual-scale fusion produces a balanced geometric representation without adding spurious artifacts.

Corner points were localized via the extremum method, and the Euclidean distance errors between the actual assembly segment (FTN13) and the target segment (FTN14) were calculated (Table 1). The results show a maximum misalignment of 51 mm at the bottom

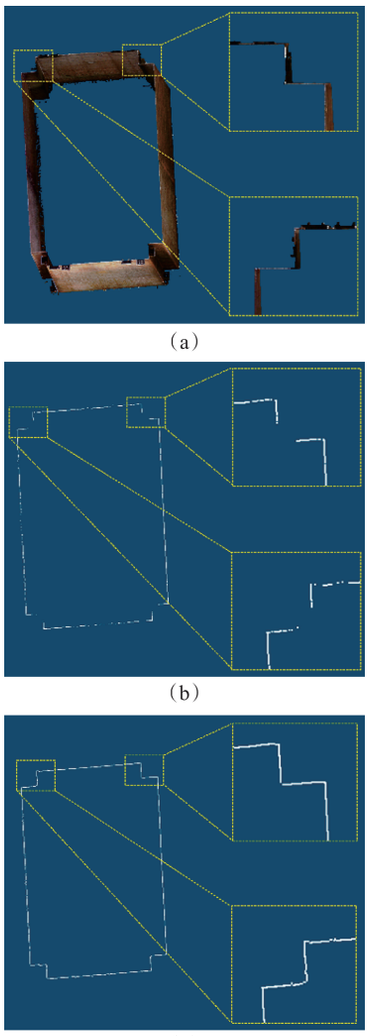

(a)

(b)

(c)

Fig. 8 Alpha-shape-based contour extraction. (a) After treatment; (b) Conventional algorithm; (c) Improved algorithm

left corner and a minimum of 5 mm at the top left corner. The error distribution reveals that assembly deviations are predominantly concentrated in the lower contact surfaces, necessitating adjustments in subsequent construction control measures.

Table 1 Corner point errors

Corner pair	Error Δ/mm
Pair 1 (bottom left)	51
Pair 2 (bottom right)	38
Pair 3 (top left)	5
Pair 4 (top right)	20

4.4 Methods comparison

To verify the performance of the proposed algorithm, three conventional algorithms were compared: the conventional Alpha-shape algorithm, Poisson reconstruction, and RANSAC-ICP. These algorithms are briefly introduced as follows.

(1) Conventional Alpha-shape algorithm: The Alpha-shape algorithm is a computational geometry approach that constructs point cloud boundaries by extending convex hull principles with an adjustable parameter to regulate structural granularity.

(2) Poisson reconstruction: Poisson reconstruction is an implicit surface generation method that recreates seamless 3D models using partial differential equations derived from the normal of an orientated point cloud.

(3) RANSAC-ICP: The RANSAC-ICP multi-stage registration architecture combines ICP for iterative geometric alignment refinement and RANSAC for robust primitive fitting.

The extracted contour data for segments FTN12, FTN13, and FTN14 were processed using the above algorithms. Their performance was evaluated using the metrics defined in Section 3.3 (Table 2). The average results across the three segments are shown in Fig. 9.

Table 2 Evaluation metrics of different methods

Extraction methods	C_{comp}/%			D_H/mm			C_{SI}/%		
	FTN12	FTN13	FTN14	FTN12	FTN13	FTN14	FTN12	FTN13	FTN14
Proposed algorithm	97.7	98.8	97.8	0.073	0.092	0.102	74.20	73.63	73.40
Conventional Alpha-shape algorithm	56.8	61.8	55.8	0.176	1.107	0.187	40.00	60.57	52.10
Poisson reconstruction	52.0	59.9	54.2	1.933	2.109	1.897	14.79	21.66	22.11
RANSAC-ICP	55.0	49.6	46.0	4.793	6.174	5.486	23.60	17.02	11.71

As shown in Figs. 9(a), (b), and (d), the improved algorithm achieves a C_{comp} of 98.1%, a D_H of 0.089 mm, and a C_{SI} of 73.74%. This performance is attributed to its multiscale α-values strategy, which incorporates density-adaptive thresholding. The method employs a parameter-switching strategy (5, 10, and 20 mm) that enables precise capture of submillimeter features in high-curvature regions, such as bolt holes, when using small α-values. In flat regions, such as chamber walls, large α-values are used to suppress noise, reducing maximum geometric deviations by over 95%. The enhanced extremum method with density-adaptive thresholds ensures a feature matching accuracy greater than 98% under complex noise conditions. Unlike Poisson global smoothing artifacts and RANSAC-ICP random sampling limitations, the proposed method preserves nonprismatic structural integrity while achieving millimeter-level engineering precision. The improved algorithm demonstrates a maximum processing capacity of 15×10^6 points (Fig. 9(c)). This improvement stems from the implementation

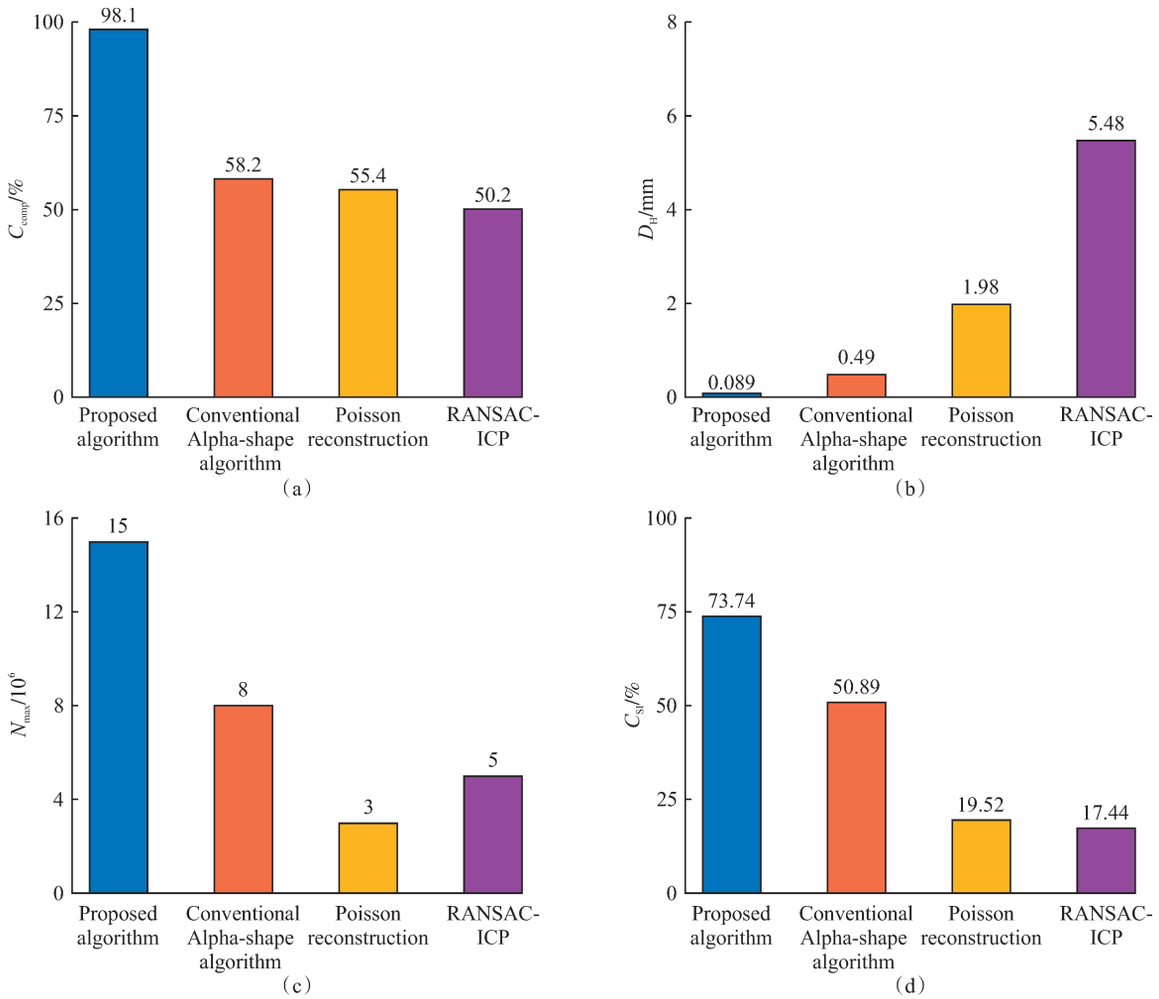

Fig. 9 Quantitative comparison of the average evaluation metrics of the improved algorithm with the mainstream technique. (a) C_{comp}; (b) D_H; (c) N_{max}; (d) C_{SI}

of KD-tree-based spatial indexing and a parallel computing architecture, which overcomes the memory and computational bottlenecks of traditional methods, increasing single-node processing capacity by a factor of 4-7.

5 Conclusions

(1) The improved Alpha-shape algorithm, which incorporates a multiscale contour extraction method based on adaptive α-selection, achieves a D_H of 0.089 mm, a C_{comp} of 98.1%, and a C_{SI} of 73.74%, indicating the effectiveness of the proposed method.

(2) The proposed method reduces point cloud data volume by 46.3%, resulting in a 210% improvement in data reduction efficiency, while maintaining a single-operation processing capacity of 15×10^6 points.

(3) Compared with Poisson reconstruction, the conventional Alpha-shape algorithm, and RANSAC-ICP, the proposed method improves C_{comp} by 42.7%, 39.9%, and 47.9%, respectively.

References

[1] ZHENG J. Recent construction technology innovations and practices for large-span arch bridges in China[J]. Engineering, 2024, 41: 110-129.

[2] YI M S, PARK J S, SEO J K. A novel pre-processing modelling method for the finite element analysis of the thermal deformation of large structures in the erection stage[J]. Ocean Engineering, 2022, 266: 112891.

[3] WANG Y C, CHEN T H, YU B, et al. Detection of road ancillary facilities considering MLS point cloud neighboring features[J]. Journal of Southeast University (Natural Science Edition), 2024, 54(6): 1530-1539. (in Chinese)

[4] REBOLJ D, PUČKO Z, BABIČ N Č, et al. Point cloud quality requirements for Scan-vs-BIM based automated construction progress monitoring [J]. Automation in Construction, 2017, 84: 323-334.

[5] ZHOU X H, LIU J P, CHENG G Z, et al. Intelligent virtual pre-assembly method for large-scale complex steel arch bridges based on point cloud data[J]. China Journal of Highway and Transport, 2021, 34(11): 1-9. (in Chinese)

[6] ZHU A Z, WANG J M, PAN W M, et al. Virtual pre-assembly technology for steel box segments based on PCL [J]. Journal of Chongqing Jiaotong University (Natural Science Edition), 2024, 43(1): 10-17. (in Chi-

nese)
[7] CHENG G, WANG J, YANG J, et al. Calculation method of 3D point cloud canopy volume based on improved α-shape algorithm[J]. Transactions of the Chinese Society for Agricultural Machinery, 2021, 52(5): 175-183. (in Chinese)
[8] WANG H C, FENG D M, WU G, et al. Three-dimensional morphology and deformation measurement of curved highway bridge based on 3D laser scanning[J]. Journal of Southeast University (Natural Science Edition), 2023, 53(5): 756-764. (in Chinese)
[9] SANTOS R C D, GALO M, CARRILHO A C. Extraction of building roof boundaries from LiDAR data using an adaptive alpha-shape algorithm[J]. IEEE Geoscience and Remote Sensing Letters, 2019, 16(8): 1289-1293.
[10] ZANG D, WANG J, ZHANG X, et al. Semantic extraction of roof contour lines from airborne lidar building point clouds based on multidirectional equal-width banding[J]. IEEE Journal of Selected Topics in Applied Earth Observations and Remote Sensing, 2024, 17: 16316-16328.
[11] ZHU L Y, HUANG X M, LUO H Y, et al. Point cloud coordinate correction methods for road surface texture index calculation[J]. Journal of Southeast University (Natural Science Edition), 2023, 53(3): 526-536. (in Chinese)
[12] CHEN M, TANG Y, ZOU X, et al. High-accuracy multi-camera reconstruction enhanced by adaptive point cloud correction algorithm[J]. Optics and Lasers in Engineering, 2019, 122: 170-183.
[13] CHEN F R, XIE F F, SUN L, et al. Point cloud segmentation algorithm based on improved Euclidean clustering[J]. IEEE Access, 2024, 12: 152959-152971.
[14] YANG L, LI Y, LI X, et al. Efficient plane extraction using normal estimation and RANSAC from 3D point cloud[J]. Computer Standards & Interfaces, 2022, 82: 103608.
[15] LIAO R X, WU T, ZHANG Y M, et al. Vision-based vessel detection for vessel-bridge collision warnings under complex scenes[J]. Journal of Southeast University (English Edition), 2024, 40(1): 33-40.
[16] CELEBI M E, CELIKER F, KINGRAVI H A. On Euclidean norm approximations[J]. Pattern Recognition, 2011, 44(2): 278-283.
[17] LIAO R X, ZHANG Y M, WANG H, et al. An effective ship detection approach combining lightweight networks with supervised simulation-to-reality domain adaptation[J/OL]. Computer-Aided Civil and Infrastructure Engineering, 2025[2025-05-19]. https://doi.org/10.1111/mice.13501.
[18] ELSHAKHS Y S, DELIPARASCHOS K M, CHARALAMBOUS T, et al. A comprehensive survey on Delaunay triangulation: applications, algorithms, and implementations over CPUs, GPUs, and FPGAs[J]. IEEE Access, 2024, 12: 12562-12585.
[19] LIAO R X, ZHANG Y M, WANG H, et al. Multi-objective optimisation of surveillance camera placement for bridge-ship collision early-warning using an improved non-dominated sorting genetic algorithm[J]. Advanced Engineering Informatics, 2026, 69: 103918.
[20] HE X P, WANG H, ZHANG Y M, et al. Revit-Midas/Civil model conversion approach and its application[J]. Journal of Southeast University (Natural Science Edition), 2021, 51(5): 813-818. (in Chinese)

基于改进Alpha-shape的超高钢桥塔点云截面轮廓提取方法研究

张一鸣，赵天浩，廖睿轩，李昊卿，王浩

（东南大学混凝土及预应力混凝土结构教育部重点实验室，南京 211189）

摘要：高精度提取复杂截面轮廓是实现超高钢桥塔虚拟预装配的关键步骤。然而，三维激光扫描数据易受制造误差、重力变形与温度变化等因素影响，难以满足精密建模需求。为克服上述问题，本文提出一种基于改进Alpha-shape的点云轮廓提取方法，以提升复杂截面轮廓重建精度。该方法采用分层处理策略对三维激光扫描点云进行预处理，结合自适应体素滤波技术以有效抑制扫描噪声，并采用最近点迭代(ICP)算法实现节段点云的精确配准。在此基础上，引入拓扑自适应阈值调节机制，实现对多尺度复杂几何边界的精细刻画，有效改善传统方法在边界模糊区域的提取不稳定性问题。结合张靖皋长江大桥塔节段的点云实测数据对该方法进行验证，并与Poisson重建、传统Alpha-shape及基于ICP的随机样本一致性(RANSAC-ICP)方法进行对比。结果表明，所提方法在轮廓提取精度和数据简化效率方面均表现优异，验证了其在复杂截面几何重建中的适用性。

关键词：超高钢桥塔；点云；轮廓提取；改进Alpha-shape算法

中图分类号：U445